Applied Energy 336 (2023) 120738

Contents lists available at ScienceDirect

Applied Energy

journal homepage: www.elsevier.com/locate/apenergy

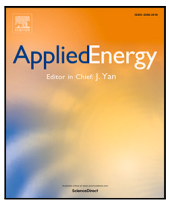

A thermodynamic-based mixed-integer linear model of post-combustion carbon capture for reliable use in energy system optimisation

Lukas Weimann [a], Guus Dubbink [a,b], Louis van der Ham [b], Matteo Gazzani [a,c,*]

[a] Copernicus Institute of Sustainable Development, Utrecht University, 3584 CS Utrecht, The Netherlands
[b] University of Twente, 7522 NB Enschede, The Netherlands
[c] Sustainable Process Engineering, Chemical Engineering and Chemistry, Eindhoven University of Technology, 5612 AP Eindhoven, The Netherlands

GRAPHICAL ABSTRACT

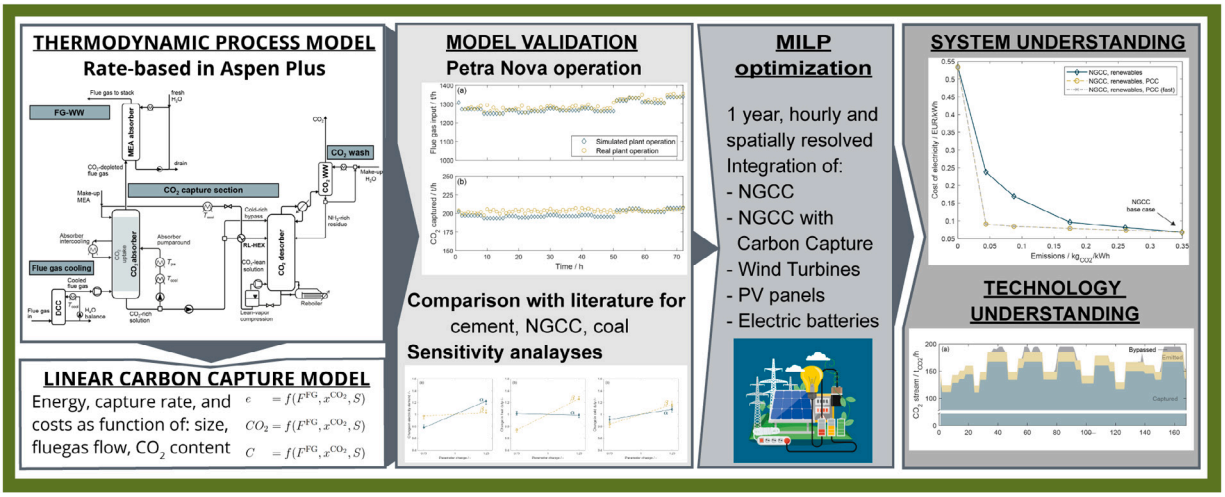

ARTICLE INFO

Keywords:
Carbon capture
MEA
Energy system
Optimisation
MILP

ABSTRACT

Assessing the role of carbon capture in energy systems dominated by non-dispatchable renewable energy sources requires a reliable and accurate model. However, carbon capture models used in complex systems optimisation are often very simplified. Therefore, we developed a mixed-integer linear model of post-combustion carbon capture starting from rigorous thermodynamic modelling in Aspen Plus. The final model decides the size and the operation of the capture process and returns the cost and energy requirements as a function of the CO_2 concentration and the flow rate of the treated flue gas. Validation against actual plant data (Petra Nova) showed excellent accuracy with a deviation in total CO_2 captured of just 2%. By applying the model to an exemplary case study, we show that it allows for co-optimising renewables deployment and carbon capture design and operation for a gas turbine, thus opening opportunities to explore new system designs of practical added value.

* Corresponding author at: Copernicus Institute of Sustainable Development, Utrecht University, 3584 CS Utrecht, The Netherlands.
E-mail address: m.gazzani@uu.nl (M. Gazzani).

https://doi.org/10.1016/j.apenergy.2023.120738
Received 7 September 2022; Received in revised form 10 January 2023; Accepted 18 January 2023
Available online 15 February 2023

Nomenclature

Acronyms

AARD	average absolute relative deviation
BAT	battery
CAR	carbon avoidance rate
CC-GT	combined-cycle gas turbine
CCS	carbon capture and storage
CCUS	carbon capture, utilisation, and storage
DCC	direct contact cooler
KPI	key performance indicator
LT	lifetime
MEA	monoethanolamine
MILP	mixed integer linear programming
NGCC	natural gas combined cycle
ODE	ordinary differential equation
PCC	post-combustion capture
PV	photovoltaic
RES	renewable energy sources
SC-GT	single-cycle gas turbine
SPECCA	specific primary energy consumption for carbon avoided
TP	transition period
WT	wind turbine
WW	water wash

Greek variables

α	performance coefficient, [MW/(kmol/s)]
β	performance coefficient, [MW/(kmol/s)]
χ	amount of cooling, heating, or electrical power, [MW]
η	efficiency, [-]
κ	cost coefficient, [MEUR/(kmol/s)]
λ	cost coefficient, [MEUR/(kmol/s)]
ν	relative ramping limit, [-]
$\Phi_{e/c}$	Objective function for emissions (e) and cost (c)
τ	time constant, [s]
θ	arbitrary vector
ε	Murphree efficiency, [-]
ζ	cost coefficient, [MEUR]

Indices

i	plant size (segment)
j	cooling, heating, or electrical power
k	type of technology
t	time

Superscripts

CO_2	CO_2 in flue gas
CAPEX	capital expenditures
FG	flue gas
max	maximum
min	minimum
S	solvent

Latin variables

$\dot{n}$	molar flow rate, [kmol/s]
$\tilde{S}$	auxiliary variable between S and a binary, [kmol/s]
a	annuity factor, [-]
C	cost, [MEUR]
CCR	carbon capture rate, [mol/mol]
e	electricity emission factor, [kg_{CO2}/kWh]
F	flow rate, [kmol/s]
$f^{O\&M}$	operation and maintenance cost factor, [-]
J_c	capital cost, [EUR/y]
J_m	maintenance cost, [EUR/y]
J_o	operation cost, [EUR/y]
LT	plant life time, [y]
Q	power integral, [MWh]
r	discount rate, [-]
S	installed flue gas flow capacity, [kmol/s]
U	imported electricity, [kWh]
u	binary, plant operation, [-]
v	binary, beginning of ramp-up, [-]
w	binary, beginning of ramp-down, [-]
x	concentration, [mol/mol]
z	binary, plant installation, [-]

1. Introduction

The role that carbon capture and storage (CCS) *should* play in the energy transition is a polarising topic of debate in both science and politics [1,2]. At the same time, the significant role it *could* play is widely acknowledged [3–5]. The arguments against CCS often tend to neglect the time factor, which is so critical for a climate-compliant energy transition, and/or ask for more efficient and cheaper capture processes, ignoring the real status of the technology and comparing it with the case of free emissions. Achieving net-zero CO_2 emissions around the year 2050 is imperative to limit global warming well below 2 °C. However, the total emitted CO_2 is even more important, i.e. the longer we continue emitting fossil-based greenhouse gases the way we used to, the faster we have to reach net-zero, and the harder the energy transition becomes [6]. Within this context, the logical approach, and likely the most time-effective, is to follow a technology-agnostic transition in which no potential solution is discarded a-priori as a matter of principle, as far as (i) it enables a timely decarbonisation and (ii) it fits with the local boundary conditions. Following this line of thought, bringing together the domains of (renewables-centred) energy system modelling and carbon capture technology modelling is certainly desirable. To do so, however, a mixed-integer linear programming (MILP) framework is required to be able to deal with the large problems (generally in the order of 10^4 – 10^6 variables [7,8], in this work ~83,000 continuous and ~14,600 integer variables) that are typical for energy system optimisations. While mixed-integer non-linear programming (MINLP) approaches have received increased attention over the past two decades [9] and solve small problems (100s of variables) in a matter of seconds [10], they quickly become hard to solve – if not intractable entirely – with increasing problem size [11]. In this case, MILP models with piece-wise linear approximations of non-linear behaviour are commonly used and shown to find feasible, and often better, solutions faster than their MINLP counterparts [11].

Some large-scale models, like TIMES [12], OPERA [13], or OSeMOSYS [14], already combine energy system modelling with carbon capture technologies but do so with constant performance indicators like efficiencies. Consequentially, they do not account for the effects of parameters like part-load operation, variations in the CO_2 concentration, or the size of the plant. That is, unless each combination of

parameters is defined as a discrete technology. However, if one aims to truly understand the role and the behaviour of a technology within a system, those features are crucial. Narrowing the focus to more detailed models, little overlap is found in the literature. Each individual domain, i.e. energy system modelling and modelling of carbon capture technologies, is undoubtedly well established and does not need to be discussed here. The interested reader can find excellent review works in the open literature, e.g. [15–17]. At their intersection, three categories can be identified: (i) CCS supply chain optimisation, (ii) optimisation of specific power and/or industrial plants with CCS, and (iii) multi-energy systems with CCS. For each of these domains, we can recognise a few important literature contributions.

If we look at chain optimisation, Zhang et al. [18,19] developed a carbon capture, utilisation and storage (CCUS) supply chain optimisation model that considers the full chain – from capture to storage – and applied it to a case study in northeastern China. They highlight that most supply chain studies are based on source–sink matching and do not include the actual capture process. While their work includes the capture process for different types of sources, they do not consider the energetic performance and the temporal resolution. A recent study from Li et al. [20], in which they apply a source–sink matching model for existing coal-fired power plants in China, reinforces the argument raised by Zhang et al.. Around the same time, d'Amore et al. performed an economic optimisation of a plausible European CCUS supply chain and included the risk analysis and mitigation measures [21] and the uncertainties in geological storage capacity [22]. Chung and Lee [23] developed a framework to derive input–output surrogate models of amine-based carbon capture processes that predict the equipment purchase cost and heating duty with good accuracy. These models are non-linear and are meant for technology screening and CCUS-focused superstructure optimisation. For large-scale system optimisation with operation decisions (i.e. they are time-discretised), however, the model's non-linear characteristics make it unsuited for the state-of-the-art mixed-integer linear programming (MILP) frameworks.

As an example for the second category, Wiesberg et al. [24] developed surrogate models for the production of bioenergy from sugarcane bagasse coupled with CCS. They did so by running factorial design experiments of the process modelled in Aspen. Basano et al. [25] modelled the integration of CCS and power-to-gas technologies with a synthetic natural gas plant. Zantye et al. [26] applied an MILP model of a flexibly operating CCS system to investigate the emission reduction from coal plants. The same team of authors also developed a stochastic optimisation approach for power plant scheduling with flexible carbon capture [27]. The model in both studies represents the CCS plant at a unit operation level and, therefore, allows optimising the plant design for a particular application. For energy system design problems on a larger scale, e.g. national or cross-sectors, this feature is usually not required as it leads to a significant increase in computational complexity.

The third category is what comes closest to the ambitions of the current work. Zhang et al. [28] embedded a power-to-methane system, fed with CO_2 captured from power generation units, into a multi-energy system providing gas, electricity and heat. Similar systems were also studied by Ma et al. [29] and Dong et al. [30], albeit with slightly different methodologies. While these three studies bring together multi-energy system models with CCS, the CCS models applied are very simplistic and/or designed for a specific application and hence cannot be generally applied to other conditions.

The list of referenced studies provides a clear representation of the types of studies that can be found in each of the three categories mentioned before. Overall, and to the best of the authors' knowledge, no model is reported in the open literature that is (a) simple enough to be used in large-scale energy system optimisation, where computation time is a crucial limiting factor, (b) detailed enough to reveal insights into the plant's operation and its effects on the rest of the system, and (c) flexible enough to have the optimisation framework choose the point-source to capture from. Therefore, the goal of this work is to fill this gap by connecting two different fields, namely that of mixed integer linear programming, which is traditionally used for control purposes or process/system optimisation, and that of separation technologies, which traditionally has roots in thermodynamics. To that end, we developed a mixed integer linear model of a post-combustion carbon capture process (based on monoethanolamine, MEA) that allows for the optimisation of size, operation, and process placement within a complex multi-energy system. Building upon a recent conference proceeding [31], we propose a new model formulation that couples thermodynamic accuracy, portability to different flue gas compositions, and scalability to different flue gas flow rates. To strike a balance between accuracy, which calls for high model fidelity, and simplicity, which is required for complex energy system optimisation, the data used to generate the carbon capture mixed integer linear model is obtained from multi-scale process simulations in Aspen Plus. The resulting energetic performance and cost of the plant are linearised as a function of the CO_2 capture capacity, the amount of flue gas to be treated at a certain time, and its CO_2 concentration. The resulting model's general formulation is framework-independent as long as the CO_2 concentration is exogenous, and it can be used for the analysis of very different systems (large/small, concentrated/diluted CO_2). It follows that the installation of the plant (yes/no), its size, and its operation pattern become decision variables of the optimisation problem, constrained and driven by system-level conditions like emission limits or available flue gas. Differently from many contributions in the field of energy/process system modelling and optimisation, we validate the model framework using real plant profiles. We, in fact, argue that the model findings, e.g. in terms of plant operation, should be similar to real plants. Finally, we provide an in-depth discussion of the model synthesis and an application example for the design of a low-carbon energy system.

To conclude, the novelty of this work can be summarised as follow:

- We provide a new mixed-integer linear model of a carbon capture process that is detailed enough to reveal operational insights but simple enough for temporally resolved assessments of complex multi-energy systems.
- The model takes the effects of part-load operation, plant size, variable CO_2 concentration and flow rate of the gas inlet on the plant performance into account.
- The model was benchmarked against real plant data, showing excellent agreement between the operation profiles.
- We show how the model can be used to derive detailed information on the design and operation of energy systems, including carbon capture and other technologies, opening doors for non-trivial optimal integrations.

The paper is organised as follows. In Section 2, the synthesis of the model is discussed. The first part covers the thermodynamic process model from which the data was generated, while the second part covers the derivation and formulation of the MILP model. In Section 3, the model is benchmarked against real operation data, and the sensitivity of the model parameters is assessed. Furthermore, the model is applied to assess the potential of decarbonising a natural gas combined cycle in the Dutch province of Zeeland. To conclude this paper, Section 4 provides a summary of the work and a discussion of the model's limitations. In the present work, the MILP formulation of the carbon capture process was implemented into a multi-energy system optimisation framework already used in previous studies of the authors [8,32].

2. Process modelling and MILP model formulation

The starting point of the carbon capture model proposed is detailed process simulations in Aspen Plus, which provide the data required to

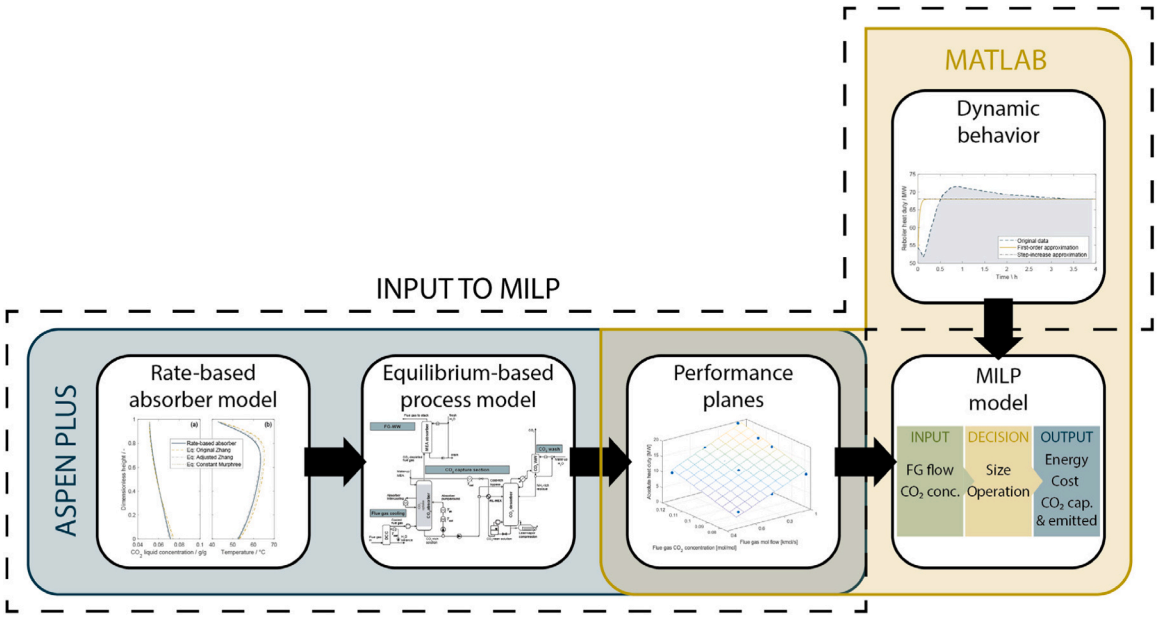

Fig. 1. Outline for deriving a process-simulation-based MILP model.

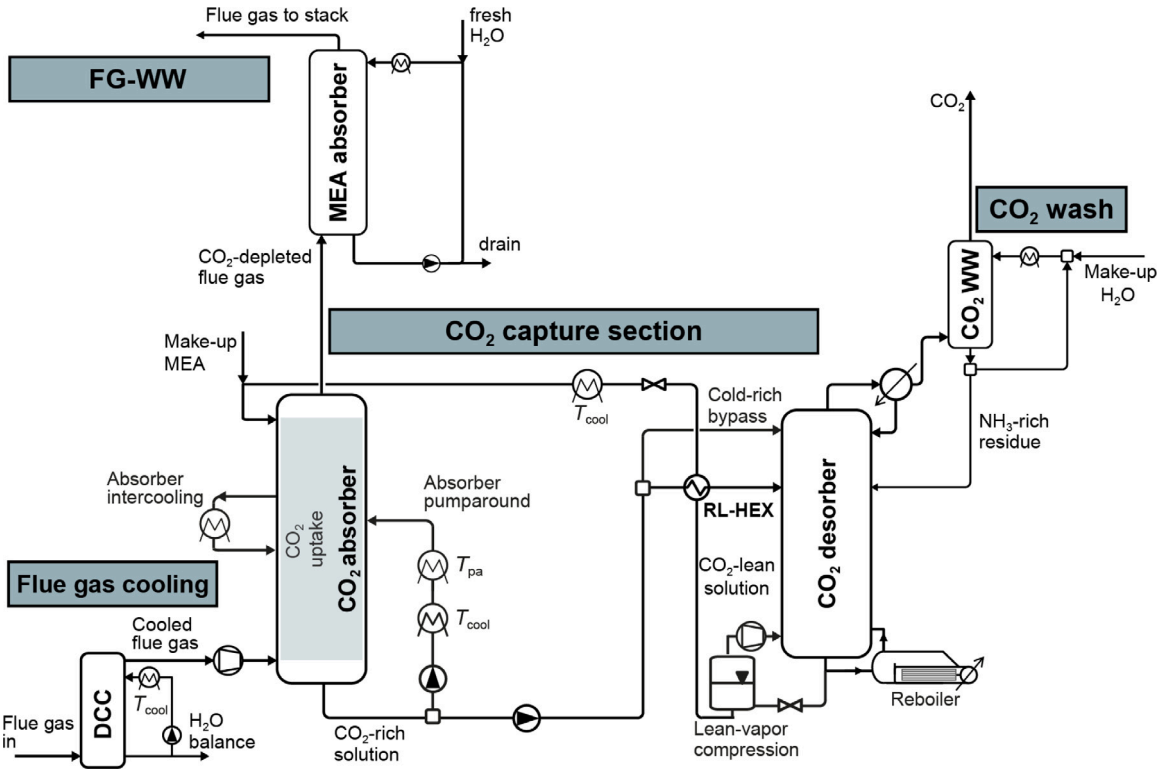

Fig. 2. Scheme of the integrated process considered in this work.

generate the linear surrogate model. The latter consists of a series of performance planes, which are dependent on the key process variables. In a parallel activity, existing dynamic data are used to generate and fit a first-order dynamic model of the carbon capture plant. The performance planes and the linear dynamics are finally combined in an MILP model and included in an existing multi-energy system optimisation framework [33]. An overview of this procedure is shown in Fig. 1; the specific building blocks are better discussed in the rest of this section.

The goal of the linear model is to obtain the key performance indicators as a linear function of the key process variables as accurately as possible. To this end, the model is generally formulated as

$$e = f(F^{FG}, x^{CO_2}, S) \quad \text{Energy (heating \& electricity)} \tag{1}$$

$$CO_2 = f(F^{FG}, x^{CO_2}, S) \quad \text{Carbon balance} \tag{2}$$

$$C = f(F^{FG}, x^{CO_2}, S) \quad \text{Cost} \tag{3}$$

where f is a linear function, F^{FG} is the flue gas mass flow, x^{CO_2} is the CO_2 concentration in the flue gas, and S is the plant size defined as the design mass flow of flue gas. The derivation of the function f is the purpose of this work. Hence, its detailed formulation will be discussed

in Section 2.5. The carbon capture rate is not listed as a variable since it is assumed to be constant at 90% for this work; note, however, that this refers to the flue gas entering the absorber and not the overall flue gas flow rate from the point source. Therefore a spectrum of carbon capture rates can be explored by the model by adjusting the treated flue gas.

In the model we propose, the heat and electricity consumption is obtained using a process modelling framework. For the dynamic and economic analyses, we use data from existing studies, but we recast them in a new linear form. More details are provided in the following.

2.1. Process modelling

The generic carbon capture process considered in this work – consisting of an absorber, stripper, heat exchangers, pumps, and a compressor – is shown in Fig. 2 and combines the standard post-combustion capture layout with state-of-the-art solutions for improved performance [34,35]. While we consider MEA as a solvent, the plant can be adapted to other solvents with minor changes.

The flue gas treated in the carbon capture process is first cooled by a direct contact cooler (DCC) and then sent to the absorber column, where CO_2 is absorbed by MEA in counter-current flow. An absorber cooling recycle is used to compensate for the exothermic absorption reaction. The CO_2-depleted top-product of the absorber is sent to a purification column, where MEA slip is reduced to ppm level and then released to the atmosphere. The CO_2-rich solution forms the bottom product of the absorber and, after heat integration, is fed to the stripper at a convenient stage. Part of the rich solution bypasses the heat integration and is fed to the top of the stripper, thus limiting the condenser duty. In the stripper, the CO_2 is released at temperatures > 90 °C and leaves the top of the column with a concentration typically larger than 95 wt%. The CO_2 product is then washed and cooled with water and sent to compression. At the bottom of the stripper, a (minor) part of the lean solvent is sent to the lean vapour compression, while the rest is sent to the absorber via heat recovery. Make-up MEA and water are added as needed, and the solvent is then ready for a new absorber cycle. Further CO_2 purification and compression of the captured CO_2 are not considered since the desired properties depend on the end-use.

As shown in Fig. 1, we use multiple levels of simulation to assess the performance of the plant and to obtain information for the linear model. The starting point is a 1-D rate-based model of the absorber in Aspen Plus; this allows us to obtain an accurate prediction of the gas–liquid profiles along the column and, therefore, reliable separation performance. However, this model is computationally expensive and cannot be implemented in a detailed carbon capture process lest accepting very long resolution times, especially when recycle streams are present. Therefore, the information of the 1-D rate-based model was transferred to the full process simulation by means of the Murphree-efficiency. To cope with deviations for varying operating conditions, the effect of flue gas flow rate and CO_2 concentration on the Murphree efficiency was assessed by simulating different off-design points with the rate-based model. The information about Murphree efficiencies and their behaviour in the off-design operation was eventually used to improve the accuracy of the integrated, equilibrium-based process model.

Rate-based absorber model. The development of a rate-based model requires a set of critical inputs, such as transport properties, column design, and kinetic models. Amirkhosrow et al. [36] have conducted a critical review of the models available in the literature and have developed a model that is able to predict liquid and gas phase CO_2 concentrations for 47 pilot plant runs within an error range of 7%. This model was used here with two adjustments: (i) Aspen Plus v10.0 was used instead of Aspen Plus v8.0 (the verification process showed no differences in the simulation results); and (ii) a column discretisation of 0.2 m per stage was used instead of 0.1 m per stage in the original study. Again, verification showed no significant deviations in the concentration and temperature profiles. The key parameters of the model are summarised in Table 1.

Table 1
Key parameters of the rate-based absorber model. * Aspen Plus definition: outlet conditions are used for the bulk of the liquid, and average conditions are used for the vapour bulk.

Property model	eNRTL
Equation of state	Soave–Redlich–Kwong
Kinetic model	Aboudheir et al. [37]
Liquid hold-up	Bravo et al. [38]
Flow model	V-Plug*
Film discretisation	Arithmetic

The Murphree efficiencies ε, which are a measure of the deviation from equilibrium for each component and stage, were retrieved from the simulations. The efficiencies were calculated for MEA, H_2O, and CO_2, while N_2 and O_2 were considered to be at equilibrium (we did not include O_2-driven MEA decomposition). Furthermore, the efficiencies are averaged per two stages for columns with more than 100 calculation stages and per five stages for columns with more than 300 calculation stages.

For the design point, D, $\varepsilon_D^{CO_2}$ can be obtained from the rate-based model's results. However, additional information is required to capture the dependency on changes in operating conditions. Zhang et al. [39] proposed Eq. (4) to correct for changes in solvent flow rate F^S, flue gas flow rate F^{FG}, and flue gas CO_2 concentration or flow rate F^{CO_2}.

$$\varepsilon^{CO_2} = \varepsilon_D^{CO_2} \frac{F_D^{FG}}{F^{FG}} \frac{F_D^{CO_2}}{F^{CO_2}} \left(\frac{F^S}{F_D^S} \right)^2 \tag{4}$$

However, in our integrated process model, the solvent flow rate is directly connected to the flue gas flow rate by fixing the absorber loading, defined as $\frac{\dot{n}^{MEA}}{\dot{n}^{CO_2}}$. Hence, the equation was simplified to account for flue gas and CO_2 flow rate only.

$$\varepsilon^{CO_2} = \varepsilon_D^{CO_2} \frac{F_D^{FG}}{F^{FG}} \frac{F_D^{CO_2}}{F^{CO_2}} \tag{5}$$

Validation of the integrated process model. To validate the equilibrium-based process model using the Murphree-efficiencies as from Eq. (5), the process results were compared against detailed pilot plant data (see experiment 2 in the supplementary material of [40]). In the reported pilot test, 51.3% CO_2 was captured from a 75.5 kg/h flue gas stream with 16.5 wt% CO_2. For both absorber and desorber, a diameter of 0.125 m and the Sulzer Mellapak 250.Y packing was used, with a packing height of 4.2 m and 2.5 m for the two columns, respectively. Moreover, the full process simulation shown in Fig. 2 was simplified to describe the experimental pilot plant. The comparison between the process model and the pilot plant data was carried out by looking at the temperature and liquid concentration profiles along the column (see Fig. 3a1–a2), as well as at the key performance parameters (see Table 2). As a measure of accuracy, the average absolute relative deviation, AARD, was calculated for the CO_2 liquid concentration profile and the temperature profile along the column.

$$AARD = \left[\frac{\sum_{i=1}^{N} \frac{\theta_i^{base} - \theta_i}{\theta_i^{base}}}{N} \right] \tag{6}$$

Here, θ_i^{base} is the ith value of the base vector (the rate-based model), θ_i is the ith value of the inspected vector (the equilibrium models with Eqs. (4) or (5)), and N is the number of values in θ.

The validation showed excellent agreement for both the temperature and the CO_2 concentration profiles, with the AARD being 1.0% and 1.7%, respectively. We can also notice that the use of Murphree-efficiency, as provided by Eq. (5), leads to results in line with the more

Table 2
Performance parameters of the pilot plant and the equilibrium-based model.

		Pilot plant [40]	Equilibrium-based model
Reboiler duty	$MJ/kg_{CO_2,cap}$	4.48	4.03
Solvent flow	kg/h	200	200
Lean loading	g/g	0.063	0.063
Capture rate	%	51.3	47.6

sophisticated rate-based approach. On the other hand, and despite the good agreement of the column profiles, the key performance indicators predicted by the process simulation deviate more significantly: the specific reboiler duty in the simulation is 10% lower than in the pilot plant, while the carbon capture rate in the simulation is 3.7 percentage points (~7%) lower than in the pilot plant. These discrepancies can be attributed to the many losses present in the pilot plant that are not included in the simulation and to the different performance in the rest of the plant (i.e. excluding the absorber). Examples include heat losses not accounted for in the simulation, different levels of heat integration in the pilot plant vs the simulation, or errors in the experimental flow rate measurements. Overall, it can be concluded that the model produces accurate column profiles and reliable, yet underestimated, specific heat duties and carbon capture rates. Given that the CO_2 capture process that we are considering in this work is significantly more complex than the experimental pilot plant and that we do not aim to constrain the process simulations with the experiment-specific performance of a pilot plant, we believe the validation results provide the needed confidence for calculation of performance maps.

Finally, we have compared the temperature and the CO_2 concentration profiles in the absorber obtained when using the rate-based model and the equilibrium models implementing (i) the original Zhang equation (Eq. (4)), (ii) the modified Zhang equation (Eq. (5)), and (iii) constant Murphree efficiencies along the column. The comparison was carried out for an off-design point where a 20% increased flue gas flow rate with respect to the on-design was applied (see Fig. 3b1–b2).

The analysis shows that the equilibrium models with Murphree efficiencies follow well the trend of the rate-based model, with also minor numerical deviation. The original Eq. (4) has an AARD of 3.3% and 1.4% for temperature and CO_2 concentration, respectively, while for the adjusted Eq. (5), these values reduce to 0.9% and 0.5%, respectively. The reason for this improvement lies in the structure of the equilibrium-based simulation, where the constant absorber loading provides a direct way to compute the solvent flow rate F^S (thus making the last term in Eq. (4) redundant).

2.2. Computation of the energy demands for the linear model

The formulation of a reliable linear model for carbon capture requires a number of performance parameters, in particular cooling, heating, and electrical power consumption. In this work, we obtain these parameters from multiple Aspen simulations using the full process simulation model described above. First, in order to cover a wide range of design sizes, three discrete plant sizes were simulated. We have selected the reference sizes by looking at existing and operating carbon capture plants. The largest one reflects the operational carbon capture plant at Petra Nova, Texas, where the capture process treats the flue gas of a 240 MW coal-fired power plant [41–43]. The absorber of this plant is 110 m high and has a nominal capture capacity of $200\,t_{CO_2}/h$. The medium size design, with an absorber height of 30 m and a nominal capture capacity of $15\,t_{CO_2}/h$, reflects the carbon capture unit of a waste incineration plant in the Netherlands [44]. Finally, small units, like they could be found for industrial boilers, were considered through the third design for a capture capacity of $7.5\,t_{CO_2}/h$; for this plant size, we do not have data from existing plants available. Second, for each of the three sizes, off-design simulations were conducted in Aspen Plus to collect operation parameters at varying flue gas flow rates and CO_2 concentrations. The flow rate was varied between 50% and 100% design capacity, assuming that the plant shuts down for lower flow rates. This assumption is based on reports from Petra Nova [42]. The CO_2 concentration was varied between 7.5 and 12.5 mol-%. For simplicity, the concentrations of oxygen and water were assumed to stay constant at 5 and 19 mol-%, respectively. Hence, the fluctuation in CO_2 was compensated by nitrogen. It is worth stressing that our linear model does not include amine degradation. Therefore, keeping the oxygen constant in the process model is a simplification that does not affect the results.

A statistical analysis of the data produced through the described simulations showed that the most relevant predictors are the total flue gas flow rate F^{FG} and the CO_2 flow rate $F^{CO_2,in}$. This confirms a physical understanding of the process: the energy requirements depend primarily on the flue gas flow rate and the amount of CO_2 captured. Since a constant capture rate of 90% is considered in this work, the CO_2 feed is a direct proxy for the flow of CO_2 captured. Accordingly, as next step, a linear relation in two dimensions (flue gas and CO_2 flow rates), i.e. a performance plane, was used to fit the performance parameter for each plant size i based on

$$\chi_{i,j} = \alpha_{i,j} F^{FG} + \beta_{i,j} F^{CO_2,in} = \alpha_{i,j} F^{FG} + \beta_{i,j} x^{CO_2} F^{FG} \quad (7)$$

where χ is the required power, j indicates the type of power (cooling, heating, or electrical power), α and β are fitting parameters, and x^{CO_2} is the CO_2 concentration as mol fraction. Note that the product of F^{FG} and x^{CO_2} is equivalent to $F^{CO_2,in}$. Fig. 4 shows the process modelling results (symbols) and the corresponding fitting using the two-dimensional projections. For simplicity, only the large-size plant is shown here, while the small and medium plants are reported in the supplementary information along with the raw data. Note that the heat duty is composed of the reboiler duty only, while the cooling duty in this model includes all heat to be removed from the system. Depending on the cooling method, the actual electricity demand associated with cooling can vary; here, we only account for the chilling duty contribution (defined as cooling below 18 °C), which roughly accounts for 3% of the cooling duty. It can be noted that the performance planes provide an excellent fit of the thermodynamic results for all plant sizes and across all tested variable ranges. However, it is worth stressing that, depending on the air excess used in the combustion (i.e. the conversion process), the CO_2 concentration can fall outside the analysed range; while it is reasonable to assume that the model predicts the performance consistently with thermodynamics, the potential for deviations should be kept in mind when applying it to very low or very high CO_2 concentrations.

2.3. Dynamic behaviour of the CO_2 capture process

Simulation and control of the dynamic behaviour of a complex process like post-combustion capture by liquid scrubbing is a challenging endeavour that requires detailed knowledge of the process design (e.g. hold-up, column thickness, heat exchanger type and area). Since the investigation and optimisation of control strategies go beyond the scope of this study and typically of energy system optimisation, this work relies on open literature to assess the dynamic behaviour. More specifically, we are interested in modelling four dynamic processes: ramp-up, ramp-down, start-up, and shut-down. The ramping processes are thoroughly discussed in [45] based on equilibrium-based Aspen Dynamics simulations for a carbon capture system with a 90% capture rate, 30% MEA solution, 13.1 kmol/h flue gas flow rate and 13.2 mol-% CO_2 concentration. The author reports the dynamic responses of CO_2 captured and energy demand for 20% ramp-up and ramp-down. As an example, the response of the reboiler heat duty in a ramp-up is shown in Fig. 5. Qualitatively, all curves behave similarly and show a transition time (the time until a new equilibrium is reached) of three hours. This is in very good agreement with dynamic experiments from the TCCS demonstration plant in Mongstad, Norway, for which a minimum transition time of three hours and a maximum recommended ramp

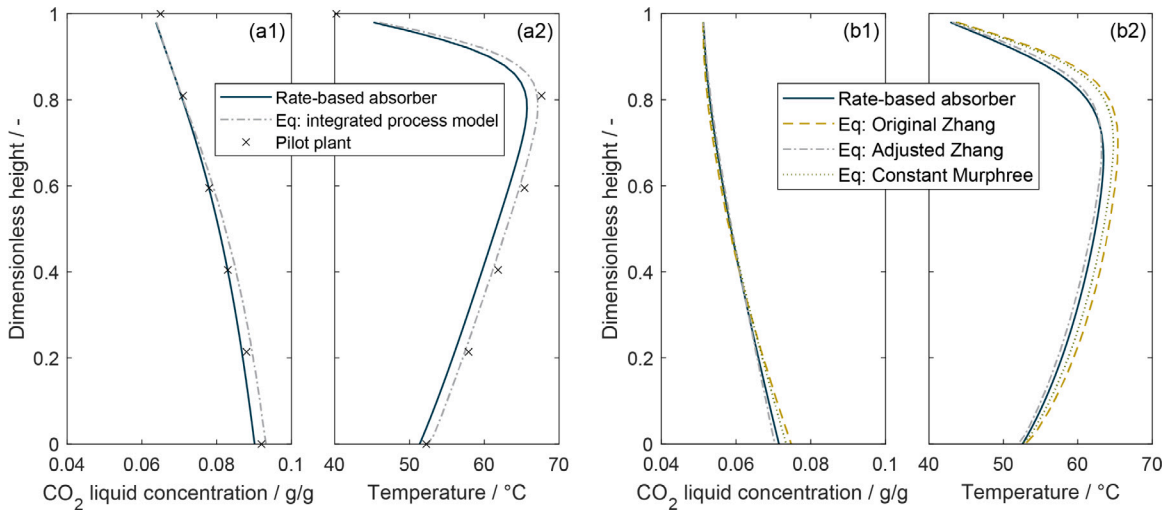

Fig. 3. CO_2 concentration and temperature profiles for the absorber column. (a1) and (a2) compare the absorber profile in an integrated process with pilot plant data and the stand-alone rate-based absorber. It is worth noting that the apparent better prediction of the integrated process model in (a2) is purely numerical and cannot be attributed to a better physical model. (b1) and (b2) show the profiles for a stand-alone absorber in off-design operation. The supplementary information provides additional comparisons of the rate-based model with the equilibrium model with Murphree efficiencies.

of 20% are reported [46]. Therefore, the data reported in [45] was linearised using a first-order ordinary differential equation (ODE)

$$\frac{\mathrm{d}Q}{\mathrm{d}t} = -\frac{1}{\tau}\left(Q - q_2\right) \tag{8}$$

where Q is the power integral, i.e. energy, transitioning from q_1 to q_2 over time t with a time constant τ and $Q = q_1$ at $t = 0$. The time constant τ is fitted to match the integral of the original power curve. As shown in Fig. 5 for the reboiler duty, the overshoot in the original power curve results in a very low time constant τ, which in turn allows simplifying the dynamic modelling by approximating the dynamic behaviour with a step increase coupled to a three-hour hold period. The errors in the total energy consumption during the transition period introduced by the two approximations are 0.17% and 0.0001% for the step increase and the first-order differential equation, respectively. It is worth highlighting that these errors only hold if the equilibration time of three hours is respected. For more frequent ramping operations, this approximation would likely lead to significant errors.

Opposed to the ramping behaviour, not much information is available for the start-up and shut-down trajectories in the open literature. Marx-Schubach and Schmitz [47] show that, counter-intuitively, the start-up time reduces with increasing target base load. Their finding also agrees with two other studies [48,49]. While a detailed discussion of this effect is beyond the scope of the current study, it is worth highlighting that start-ups to 50% base load and more take less than three hours. Therefore, and due to a lack of better information, the start-up is modelled like the ramping trajectories, i.e. a step increase and a three-hours hold time but no limitation to 20% of the design capacity. Shut-downs are assumed to occur instantaneously.

2.4. Computation of the economic performance for the linear model

Similar to the case of the dynamic behaviour, determining the costs of a plant is complex as it requires detailed knowledge of the process equipment and their associated cost. Such design and analysis are outside the scope of this work. Therefore, we decided to use the open literature as a data source for cost. It is worth stressing that our model aims to be generic and can therefore be updated with any economic input data. For this work, we refer to the work of Hasan et al. [50] (cost year 2009), who conducted an optimisation-based study for MEA as the solvent, 90% carbon capture rate, flue gas flow rates between 0.1 and 10 kmol/s, and CO_2-concentrations between 1% and 70%. Despite being ten years old, the data shows good agreement with more recent studies (+9.5% compared to [51] and −6.8% compared to [52]). Contrary to the present work, the work of Hasan et al. includes compression of the captured CO_2 to 150 bar. Hence, using the cost data provided therein provides a slightly conservative estimate for the present work.

While the authors provide a non-linear cost function in their original work, we used their raw data to fit a piece-wise linear model. The CAPEX of a post-combustion carbon capture plant, c^{CAPEX}, is a complex function of many parameters but depends mostly on (i) the flue gas flow rate design capacity S, which determines the equipment size on the absorber-side of the process, and (ii) the maximum amount of CO_2 captured $F^{\mathrm{CO_2,max}}$, which determines the equipment size on the desorber-side of the process. We can therefore define the generic equation

$$C^{\mathrm{CAPEX}} = \zeta + \kappa S + \lambda F^{\mathrm{CO_2,max}} \tag{9}$$

For a fixed carbon capture rate, CCR, this equation can be rewritten as

$$C^{\mathrm{CAPEX}} = \zeta + \kappa S + \lambda S x^{\mathrm{CO_2}} CCR \tag{10}$$

Note that Eq. (10) is bilinear with respect to S and $x^{\mathrm{CO_2}}$. Hence, this formulation can only be used if the CO_2 concentration is not a decision variable in the optimisation. The resulting linear piece-wise fitting of the source cost data proved to be very accurate; more details about the fitting are provided in the supplementary material.

2.5. Synthesis of the MILP model

Using the information presented throughout Sections 2.1–2.4, an MILP model was developed that allows for optimising the carbon capture plant size and time-discretised operation for given time-discretised flue gas availability and CO_2 concentrations. This is done by assessing the cost of the unit, the required energy (electricity, heating, and electricity associated with chilling), the amount of flue gas treated, and the resulting CO_2 emitted. Since the model is piecewise-continuous, the three simulated plant sizes are used to represent three different size segments. The limits of these segments are reported in Table 3.

The total annual costs C are defined as

$$C = \left(a + f^{\mathrm{O\&M}}\right) \sum_i \left[\zeta_i + \kappa_i S + \lambda S \max\left(x_t^{\mathrm{CO_2}}\right) CCR\right] z_i \tag{11}$$

$$= \left(a + f^{\mathrm{O\&M}}\right) \sum_i \left[\zeta_i z_i + \tilde{S}_i^z \left(\kappa_i + \lambda \max\left(x_t^{\mathrm{CO_2}}\right) CCR\right)\right] \tag{12}$$

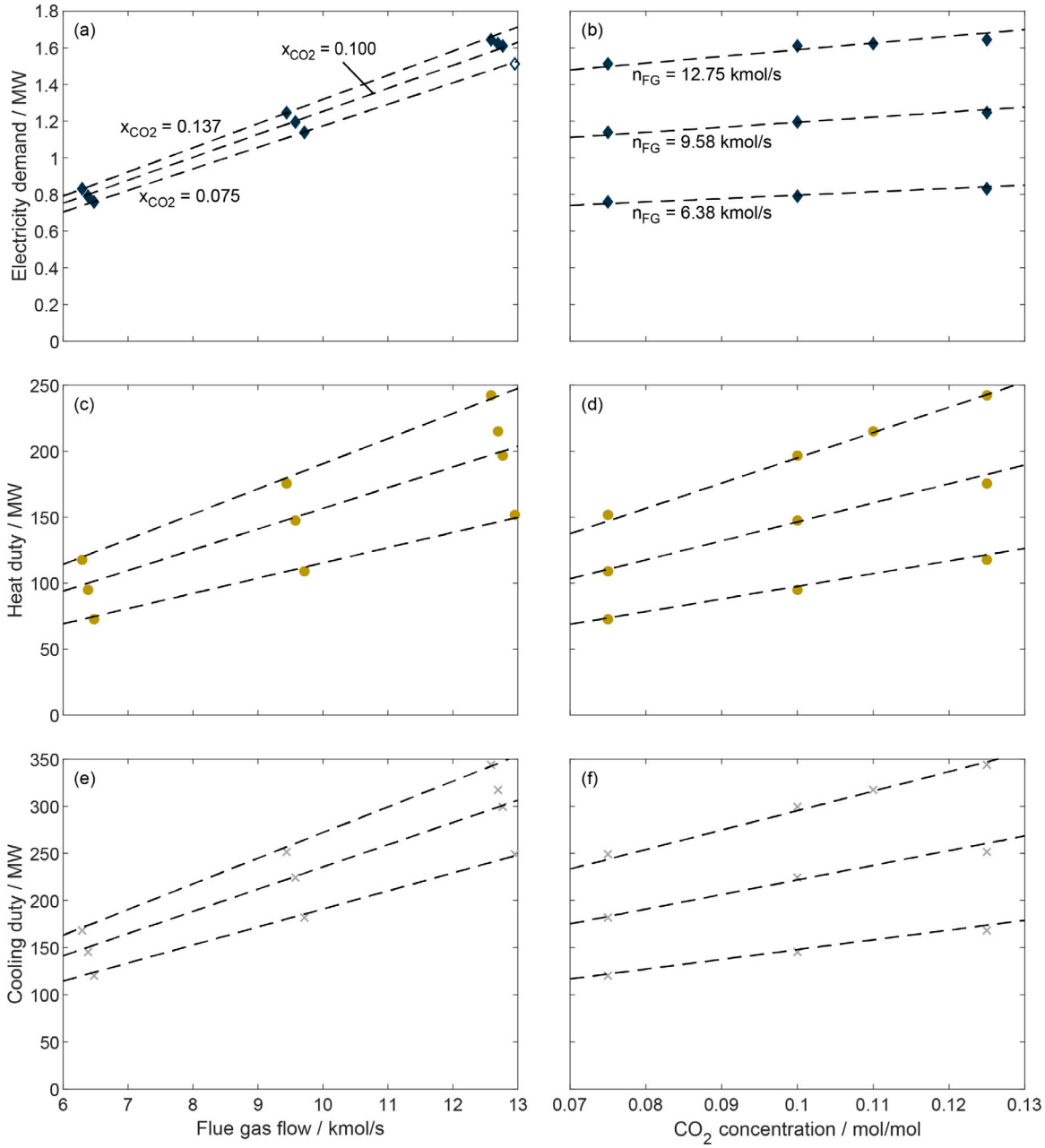

Fig. 4. 2D projections of the performance planes for electricity, heat, and cooling for a large-scale plant. The lines represent constant CO_2 concentrations (a,c,e) and constant flue gas flow rates (b,d,f), respectively.

where S is the installed capacity in terms of flue gas flow rate, z_i is a binary variable selecting the active size segment i, $x_t^{CO_2}$ is the CO_2 concentration at time t. ζ_i, κ_i, and λ_i are the cost parameters, $f^{O\&M}$ is the fraction of CAPEX included as operation and maintenance cost, and a is the annuity factor. $\tilde{S}_i^z$ is an auxiliary variable to circumvent the bilinearity between S and z_i as proposed in [53] through the constraints

$$S_i^{\min} z_i \le \tilde{S}_i^z \le S_i^{\max} z_i \tag{13}$$

$$S - S_i^{\max}(1 - z_i) \le \tilde{S}^z \le S \tag{14}$$

where $S_i^{\min}$ and $S_i^{\max}$ are the lower and upper limits of the size segments. Furthermore, only one segment can be selected at a time

$$\sum_i z_i \le 1 \tag{15}$$

The installed capacity S is constrained to be 0 if the size segment i is not installed ($z_i = 0$) and between the minimum $S_i^{\min}$ and maximum $S_i^{\max}$ of the selected size segment otherwise

$$\sum_i z_i S_i^{\min} \le S \le \sum_i z_i S_i^{\max} \tag{16}$$

The flue gas flow rate is then constrained to be 0 if the unit is turned off at time instance t (defined through another binary $u_{t,i} = 0$) and between 50% and 100% of the installed design capacity S otherwise

$$0.5\tilde{S}_{i,t}^u \le F_{i,t}^{FG} \le \tilde{S}_{i,t}^u \tag{17}$$

Again, $\tilde{S}_{i,t}^u$ is the auxiliary variable used to represent the product of S_i and $u_{i,t}$. Since the statistical analysis of the energy performance data showed no significant effect of the plant size within a specific size segment, Eq. (7) is considered to be valid across the whole range for each size segment. Therefore, a time-resolved equivalent of this equation is

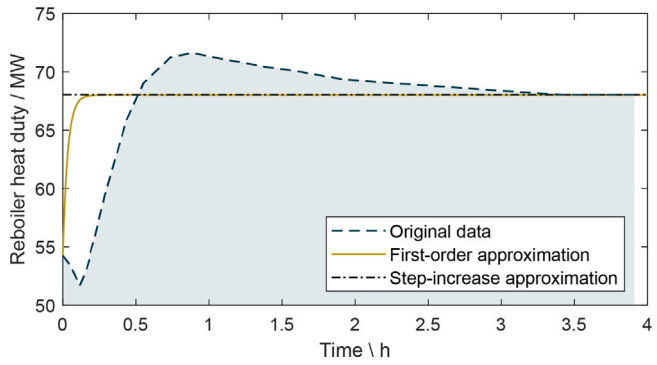

Fig. 5. Dynamic response of the reboiler heat duty to a 20% ramp-up at t=0. For comparison, the corresponding first-order approximation and step-increase approximation are shown.

used directly in the model to calculate the energy requirements as

$$\chi_{j,t} = \sum_i \chi_{i,j,t} = \sum_i F_{i,t}^{\mathrm{FG}} \left(\alpha_{i,j} + \beta_{i,j} x_t^{\mathrm{CO_2}} \right) \tag{18}$$

Here, a binary to select the proper size segment is not necessary since $F_{i,t}^{\mathrm{FG}}$ is constrained to be 0 for non-selected segments according to Eq. (17).

The amount of CO_2 captured, $F_t^{\mathrm{CO_2},cap}$, and the CO_2 emitted, $F_t^{\mathrm{CO_2},emit}$, are therefore defined as

$$F_t^{\mathrm{CO_2},cap} = 0.9 x_t^{\mathrm{CO_2}} \sum_i F_{i,t}^{\mathrm{FG}} \tag{19}$$

$$F_t^{\mathrm{CO_2},emit} = 0.1 x_t^{\mathrm{CO_2}} \sum_i F_{i,t}^{\mathrm{FG}} \tag{20}$$

To describe the dynamic behaviour of the technology, as discussed in Section 2.3, a set of five constraints is required. First, two binary variables identify the beginning of a ramp-up or ramp-down event – $v_{i,t}$ and $w_{i,t}$, respectively – and need to be constrained as

$$F_{i,t+1}^{\mathrm{FG}} - F_{i,t}^{\mathrm{FG}} \leq v_{i,t} S_i^{\max} \tag{21}$$

$$F_{i,t}^{\mathrm{FG}} - F_{i,t+1}^{\mathrm{FG}} \leq w_{i,t} S_i^{\max} \tag{22}$$

These constraints force $v_{i,t} = 1$ if the flue gas flow increases and $w_{i,t} = 1$ if the flue gas flow decreases in time instance $t+1$. To ensure that they are mutually exclusive and that no other ramping event starts within the transition period TP, we formulate the following constraint

$$\sum_{p=0}^{TP} \left(w_{i,t+p} + v_{i,t+p} \right) \leq 1 \tag{23}$$

Furthermore, we constrain the ramping limits for the ramp-down operation as

$$F_{i,t}^{\mathrm{FG}} - \nu S - (1 - u_{i,t+1}) S_i^{\max} \leq F_{i,t+1}^{\mathrm{FG}} \tag{24}$$

and for the ramp-up operation as

$$F_{i,t+1}^{\mathrm{FG}} \leq F_{i,t}^{\mathrm{FG}} + \nu S + (1 - u_{i,t}) S_i^{\max} \tag{25}$$

Here, ν is the ramping limit as a share of installed capacity. The terms $(1 - u_{i,t}) S_i^{\max}$ and $(1 - u_{i,t+1}) S_i^{\max}$ allow for the ramping to be unconstrained in case of a start-up or a shut-down since an instantaneous shut-down and a very fast start-up were assumed (see Section 2.1). The carbon capture rate of 90% is assumed to remain constant during the ramping process.

Finally, all binary operation variables are constrained to be 0 if the unit is not installed

$$0 \leq u_{i,t} \leq z_i \tag{26}$$

$$0 \leq v_{i,t} \leq z_i \tag{27}$$

$$0 \leq w_{i,t} \leq z_i \tag{28}$$

The values of all parameters used in Eqs. (12)–(28) are reported in Table 3.

3. MILP model validation and application to energy system optimisation

3.1. Comparison with experimental data from Petra Nova

A significant limit of linear models for energy system optimisation is that they are hardly validated with real plant data or detailed process models; often, they are very simplistic, and the comparison would be pointless. Here, we follow a different approach, and we assess the accuracy of the linear model proposed by comparing it against the actual operational data of the Petra Nova plant [41]. We indeed argue that the optimal MILP model outcome should be in line with the data of a plant designed thanks to thousands of engineering working hours. The published data nicely report the absolute captured CO_2 and the capture rate for a 72 h window. Since the public data is not evenly distributed but ranges from sub-hourly to multi-hourly, linear interpolation was used to derive an hourly distributed profile (with good agreements between the two, see supplementary information for details). The flue gas flow rate, while not being published explicitly, could be calculated from the aforementioned data sets assuming a constant flue gas composition (19 wt-% CO_2), which is in line with boiler operation in large coal power plants. For setting up the validation process, the hourly derived flue gas flow rate of Petra Nova was used in the model as an upper limit for the flue gas feed to the PCC unit. To replicate the profile as closely as possible, the model was set to minimise the CO_2 emissions by deciding (i) the PCC design size, and (ii) its operation, the latter via varying the flue gas feed to the PCC unit. The results of the comparison between the real data and the model are shown in Fig. 6. Overall, the treated flue gas and the resulting CO_2 capture are in good agreement with the plant data in terms of both magnitude and profile in time; in other words, when minimising emissions, the carbon capture MILP model chooses to treat the same amount of flue gases of the Petra Nova capture plant and follows the same operation in time. It can, in fact, be noted that the model mimics the increase in flue gas flow rate after 50 h of operation. At the same time, the modelled flue gas flow rate pattern clearly shows the effect of the constrained dynamics: steady-state operation is maintained for at least three hours after each ramping operation, causing some of the available flue gas to be bypassed. It can also be noted that the CO_2 captured is slightly underestimated during the first ~50 h. The reason for this lies in the difference between the varying carbon capture rate of the real plant (dropping from 93.6% to 87.6%) and the constant carbon capture rate of 90% in the model. Nevertheless, the total CO_2 captured over the analysed period deviates by only 2% and the increasing trend in time is correctly reproduced.

3.2. Comparison with literature data outside of the calibration range

The model was developed based on Aspen simulations spanning a CO_2 concentration range from 7.5 mol% to 12.5 mol%. This, however, does not cover all potential CCS application cases. On the lower side, one can find combined-cycle flue gas with a concentration of around 4 mol%. On the higher side, cement plants exceed the calibrated range with > 18 mol%. To show that the thermodynamic foundation of the framework allows using the model outside the calibration range (i.e. extrapolating) with confidence, we compared the model outcome with studies from the open literature. To do so, we fed the developed model with the CO_2 concentration and flue gas flow rate of the reference processes. The energetic performance was then compared with the data reported in the respective studies. The results are shown in Table 4. It is important to note that the reported values do not include the

Table 3
Numeric values of the model parameters.

Real-world example		Small Industrial boiler	Medium Waste incineration [44]	Large Power plant [43]
$f^{O\&M}$	[%]	5	5	5
r	[%]	10	10	10
LT	[y]	30	30	30
ν	[-]	0.2	0.2	0.2
TP	[h]	3	3	3
$\dot{S}^{min}$	[kmol/s]	0.0895	1	5
$\dot{S}^{max}$	[kmol/s]	1	5	12.53
Cost				
ζ	[MEUR]	2.17	11.1	10.8
κ	[MEUR/(kmol/s)]	3.44	2.83	3.11
λ	[MEUR/(kmol/s)]	185	125	123
Electricity				
α	[MW/(kmol/s)]	0.0937	0.0945	0.0958
β	[MW/(kmol/s)]	0.2719	0.2787	0.2885
Heat				
α	[MW/(kmol/s)]	−0.6068	−1.240	0.2684
β	[MW/(kmol/s)]	158.71	175.32	150.22
Cooling				
α	[MW/(kmol/s)]	4.399	4.215	6.951
β	[MW/(kmol/s)]	186.0	199.0	162.1

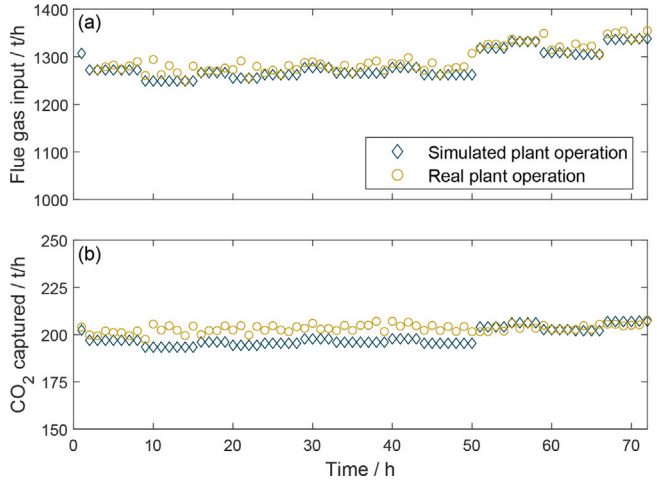

Fig. 6. Comparison of real operation data from Petra Nova [41] and the model output for (a) flue gas flow rate fed to the PCC plant and (b) CO_2 captured.

compression energy to make for a fair comparison. Furthermore, it has to be highlighted that a linear, extrapolated model is compared with results of detailed process modelling. Hence, the aspiration is not to achieve perfect reproduction but reasonable agreement.

Across all comparison cases, the electricity consumption is underestimated using the model presented in the current work. However, a wide range of values for electricity consumption can also be found among the comparison cases themselves. This suggests that the electricity consumption is highly dependent on underlying assumptions like blower efficiencies and exact system boundaries, i.e. the list of auxiliaries, which cannot be included in a linear model. Consequentially, the predicted heating duty and cooling duty is more accurate than the predicted electricity demand. Moreover, the predictions for large-scale plants (NGCC and coal) are better than for smaller plants (cement). Finally, the difference in heating duty between the two IEA cement cases, which originates from a difference in absorber loading, is not reproduced by the linear model. This was to be expected since the linear model does not include absorber loading as a variable. However, the model shows the desired behaviour by predicting a value that lies well between the two IEA cases.

3.3. Model sensitivity towards the input performance curves

The modelling of technologies comes with inherent uncertainties — an effect that is amplified if said model is linearised. To evaluate the effect of uncertainties in the parameters of the performance model, each of the parameters was varied individually by +25% and −25% while also considering different energy conversion technologies as a source of CO_2 (and therefore different energy and heat availability). Consequently, we assessed both the resulting change in performance and the PCC key performance indicators (KPIs), i.e. carbon avoidance rate (CAR) and specific primary energy consumption for carbon avoidance (SPECCA). We defined the CAR as

$$CAR = 1 - \frac{F_{CO_2}^{emitted}}{P_{net}} \frac{P_{net}^{ref}}{F_{CO_2}^{emitted,ref}} \tag{29}$$

where P_{net} is the net electrical power output, and the superscript 'ref' refers to the reference scenario, i.e. the scenario without post-combustion capture. The SPECCA was defined as

$$SPECCA = \frac{\frac{1}{\eta_e^{eff}} - \frac{1}{\eta_e^{ref}}}{\frac{F_{CO_2}^{emitted,ref}}{P_{net}^{ref}} - \frac{F_{CO_2}^{emitted}}{P_{net}}} \tag{30}$$

where η_e is the electric efficiency and the superscript 'eff' indicates the effective efficiency, i.e. net power output over primary energy input. Finally, the electricity-specific CO_2 emissions complement CAR and SPECCA.

To pick appropriate scenarios for this sensitivity analysis, three aspects are important: (i) The effects of the performance parameter variation should be isolated from any other effects that could distort the outcome. Therefore, a focus is put on the energetic performance of the plant, as the economic performance depends on many exogenous assumptions, e.g. utility prices. (ii) The scenarios should feature different flow rates and CO_2 concentrations to capture the effect of tilting the performance curves (i.e. varying α and β). (iii) The scenarios should vary in the amount of available off-heat, as this affects the SPECCA.

To this end, three different conversion technologies were selected: a simple cycle gas turbine (SC-GT), a combined cycle gas turbine (CC-GT), and a coal-fired power plant. These conversion technologies vary in terms of the available off-heat, the CO_2 concentration in the flue gas and the amount of flue gas. To further amplify the latter, each conversion technology was considered at 50 MW and 100 MW, resulting in a total of six different scenarios. It should be noted that the purpose

Table 4
Comparison of model results with literature data for designs outside the calibrated CO_2 concentration range. The difference between *IEA(a)* and *IEA(b)* is the absorber loading.

		CEMCAP [54]	IEA(a) [55]	IEA(b) [55]	CAESAR(a) [56]	CAESAR(b) [56]
Application		cement	cement	cement	NGCC	coal power
CO_2 concentration	[mol/mol]	0.18	0.18	0.18	0.04	0.14
Flue gas flow rate	[kmol/s]	3.55	7.00	7.00	23.4	27.0
Original Study						
Capture rate	[–]	0.900	0.946	0.946	0.905	0.890
Electricity demand	[MJ/kg_{CO2}]	0.142	0.076	0.076	N/A	0.146
Heating duty	[MJ/kg_{CO2}]	3.83	3.38	4.83	3.96	3.73
Cooling duty	[MJ/kg_{CO2}]	4.91	N/A	N/A	N/A	3.85
Model						
Capture rate	[–]	0.90	0.90	0.90	0.90	0.90
Electricity demand	[MJ/kg_{CO2}]	0.020	0.021	0.021	0.068	0.025
Heating duty	[MJ/kg_{CO2}]	4.25	3.83	3.83	3.96	3.84
Cooling duty	[MJ/kg_{CO2}]	5.62	5.07	5.07	8.52	5.37

Table 5
Technology assumptions for the scenarios used in the sensitivity analysis.

		SC-GT	CC-GT	Coal	Gas boiler
Electric efficiency	[kW_e/kW_{fuel}]	0.35	0.6	0.4	0
Heat efficiency	[kW_h/kW_{fuel}]	0.52	0	0	0.9
Emission factor	[kg_{CO2}/kWh_e]	0.198	0.198	0.342	0.198
CO_2 concentration	[mol_{CO2}/mol_{fuel}]	0.4	0.4	0.15	N/A

of this analysis is not to rank the considered processes but to illustrate the effect of uncertainties of the model for the selected examples. The key assumptions used to derive these scenarios are summarised in Table 5. The detailed results of the sensitivity analysis, including a tabulation of all experiments, are provided in the supplementary material.

The aforementioned variations in scenarios and parameters resulted in a total of 114 different sensitivity experiments. Fig. 7 shows the effect of varying the performance parameters on electricity consumption, heat duty, and cold duty across all experiments (note that we quantify the sensitivity in relative terms, i.e. relative change in independent variable per relative change in parameter). The span of values resulting from variations of other parameters (flue gas flow rate and CO_2 concentration) are displayed as vertical bars. As this span is very narrow, the found sensitivity is quite independent of those other parameters. The electricity consumption shows a sensitivity of about 0.8 towards α, while hardly any sensitivity can be observed towards β. This indicates that the flue gas flow rate is the main driver of electricity consumption and agrees with expectations as it originates from pumps, blowers, and compressors, which in turn scale with the total amount of gas treated. The heat duty's sensitivity shows the opposite picture: a sensitivity of about 1 towards β and hardly any sensitivity towards α. Again, this agrees with expectations since the heat duty (in terms of power) depends mostly on the amount of CO_2 captured and, therefore, on the amount of CO_2 fed for a constant carbon capture rate. The cold duty's sensitivity lies between electricity and heat for both parameters. Its sensitivity towards α is about 0.4 and towards β about 0.7. When interpreting this analysis, it has to be kept in mind that heat is the most significant contributor to the total energy requirement. Considering that variations in β affect heat and cold duty the most, particular attention needs to be paid to properly assess the value of this parameter. Conversely, variations in α only affect the electricity demand to a significant extent, whose contribution to the total energy requirement is minor. Hence, the effects of uncertainties in α are much less severe.

The sensitivity of the energy performance translates differently into the sensitivity of the KPIs for different applications. Fig. 8 shows the variation in CAR, SPECCA, and electricity-specific CO_2 emissions for the three different conversion technologies. The variation shown in the figure is a collection of all varied parameters, i.e. model parameters for electricity consumption, heat duty, and cold duty, but also flue gas flow rate and available off-heat. The CO_2 concentration, being specific for a conversion technology, is constant within one data set. The bars in Fig. 8 show the total spread of values, while the dark lines show one standard deviation assuming normal-distributed data.[1] The KPI most affected by variations in the input parameters is the SPECCA, followed by the specific CO_2 emissions and lastly, the CAR. Looking at different conversion technologies, the KPIs of coal are most affected, followed by CC-GT and, lastly, SC-GT. The reason why SC-GT is least affected is the abundance of heat available. Therefore, changes in heat duty can be compensated easily. Note that this changes significantly if the heat produced by the SC-GT is not freely available but dedicated to a different end-use. The changes in specific CO_2 emissions and CAR are not visible in Fig. 8. Neither CC-GT nor coal-fired power plants are assumed to have useable waste heat. For simplicity, we consider that any heat required by the carbon capture plant is supplied via gas boilers (see the last column in Table 5 for boiler input data); The exact plant configuration depends on several exogenous variables, e.g. prices and CO_2 constraints, that are not assessed in this sensitivity analysis of the model. Ideally, the flue gas of those boilers would be treated in a PCC plant as well. For this analysis, however, we assumed that the gas boilers emit their flue gas unabated, hence affecting the CAR. The slightly lower sensitivity of the CC-GT plant's KPIs compared to the coal ones can be explained by the difference in the flue gas produced. Coal-fired power plants produce a significantly higher CO_2 concentration, hence amplifying the relative importance of variations in β. In other terms, treating flue gas from coal-fired power plants requires more heat per flue gas treated. Hence, it is more affected by uncertainties of the heat duty.

3.4. Application of the model to an energy system design

In the previous sections, we have described the model foundations and the model equations, and we have validated the accuracy with real plant data. Moreover, we have shown how the model behaves when varying the input parameters. Here, we aim to demonstrate the use of the model for its intended purpose, i.e. a large-scale energy/process system design and optimisation. More specifically, we aim to investigate the decarbonisation potential of a generic energy system that relies on fossil fuels for electricity energy supply, here chosen to be a natural gas combined cycle (NGCC, the state-of-the-art in natural gas-based electricity generation). The scope is to show the model's potential in revealing the optimal integration of CCS with an NGCC plant, renewable energy technologies, and batteries. As an exemplary case, the analysis

[1] Since the data is not truly normal-distributed, the standard deviation should be considered as indicative value only.

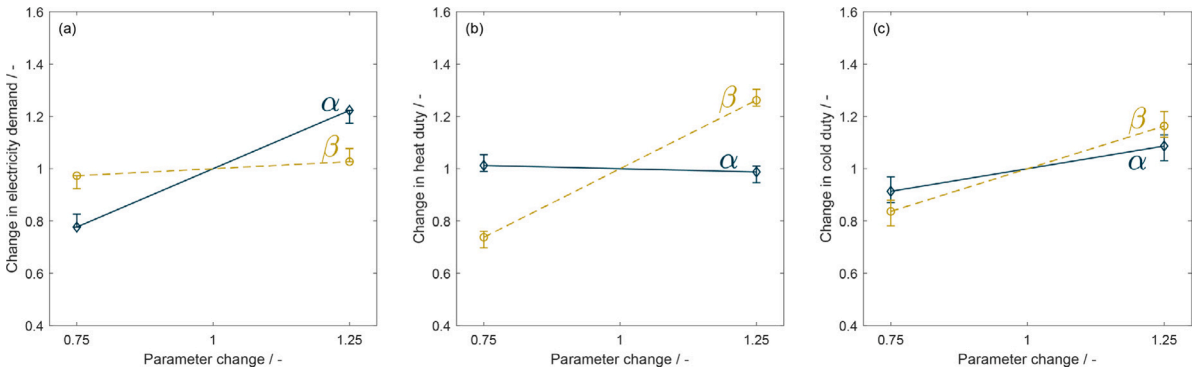

Fig. 7. Effect of the variation of the model parameters on the model's energetic performance: (a) electricity consumption, (b) reboiler heat duty, (c) cooling duty. The vertical bars show the effect of also varying the CO_2 concentration and the flue gas flow rate.

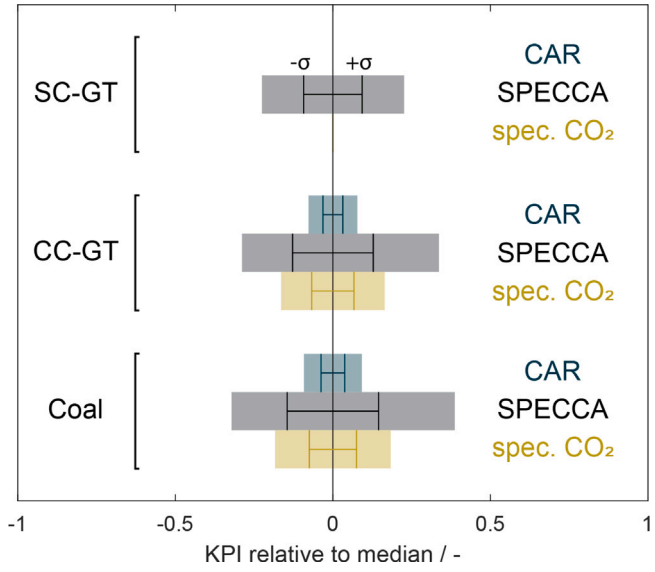

Fig. 8. Effect of the variation of model parameters on KPIs. The bars show the total spread of data, and the dark lines show one standard deviation assuming normal-distributed data. *spec.* CO_2 refers to the electricity-specific CO_2 emissions of the total process.

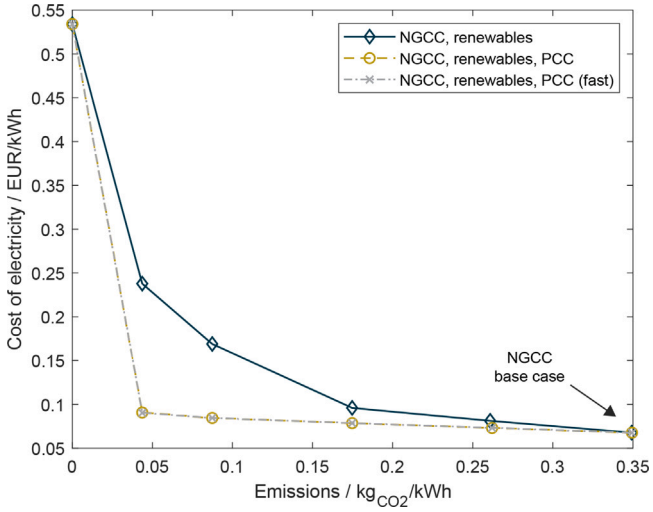

Fig. 9. Pareto-optimal designs with respect to cost and CO_2 emissions for different sets of technologies.

is based on electricity demand and weather data of the Dutch province of Zeeland for the year 2019 (population: 383'000, size: 2934 km^2, electricity demand: 3225 GWh/y). All analyses were conducted using the multi-energy system optimisation framework [8,32] and the time-hierarchical method presented by the authors in earlier work [57]. The objective functions are the total annual system cost, Φ_c, and the annual system-wide CO_2 emissions, Φ_e. The annual system cost are made up of the annual capital cost, J_c, the annual operation cost, J_o, and the annual maintenance cost, J_m.

$$\Phi_c = J_c + J_o + J_m \tag{31}$$

The emissions are made up of the imported electricity and the net production of CO_2 within the system

$$\Phi_e = \sum_t \left(eU_t + \sum_k \left(F_{k,t}^{CO_2,out} - F_{k,t}^{CO_2,in} \right) \right) \tag{32}$$

where e and U are the emission factor and amount of imported electricity, respectively, and k indicates the different technologies — in this particular work NGCC and PCC. A detailed explanation of the framework and solution method is beyond the scope of this work, and the interested reader is referred to the respective literature. The key assumptions and data relevant to this case study are summarised in Table 7.

We conducted four different steps in this assessment. First, the size and operation of an NGCC are optimised for costs under the constraint that it supplies the end-user demand. This represents a plausible state-of-the-art non-decarbonised energy system. The identified NGCC size is fixed for all subsequent simulations. In a second step, we extend the set of technologies by wind turbines, photovoltaics, and batteries to investigate the renewables-based decarbonisation potential. To obtain a Pareto front in the cost-CO_2 emissions plane, the new system is optimised for cost while being subject to different emission limits. In the third step, we apply the same emission limits as in the second step, but we extend the set of available technologies to include CCS, i.e. the decrease in emissions must be as when integrating renewables and batteries, but it can also be achieved deploying CCS. To compensate for any electricity production losses due to the PCC unit and avoid infeasibility, we allow for electricity import with a specific cost and emission factor equal to what was found for the NGCC in the first step. Finally, in a fourth analysis, we repeat step three, relaxing the constraints on the dynamic behaviour of the PCC unit: the transition period, TP, was set to 1 h. This allows us to explore what the competitive advantage of a more flexible CCS technology would be. Table 6 summarises the characteristics of the four analyses.

Fig. 9 shows the cost of reducing emissions in the different analyses listed above. The lines are Pareto fronts, i.e. they report the minimum cost required for a specific emission reduction, and the area below

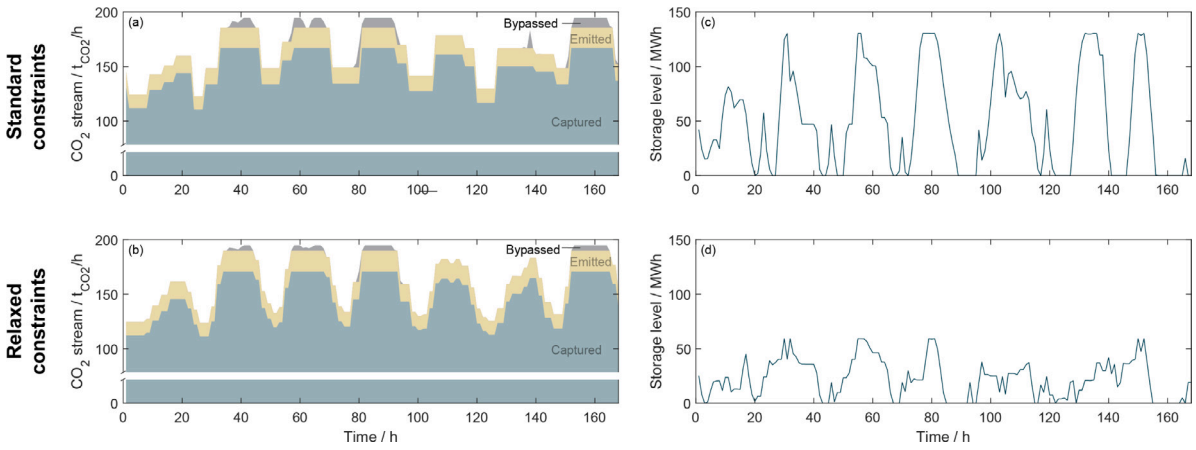

Fig. 10. Effect of relaxing the constraints on the PCC's dynamics for the first week of the analysed year. (a)–(b) CO_2 balance for standard constraints and relaxed constraints, respectively. (c)–(d) battery operation for standard constraints and relaxed constraints, respectively.

Table 6
Summary of the analyses conducted for the case study.

	Analysis 1	Analysis 2	Analysis 3	Analysis 4
Obj. function	min cost	min cost	min cost	min cost
CO_2 emission limit kg/kWh	–	[0, 0.044, 0.087, 0.1755, 0.262, 0.349]	[0, 0.044, 0.087, 0.1755, 0.262, 0.349]	[0, 0.044, 0.087, 0.1755, 0.262, 0.349]
Technologies	NGCC	NGCC, PV, WT, BAT	NGCC, PCC, PV, WT, BAT	NGCC, PCC ($TP = 1$), PV, WT, BAT
Decision variables	design of NGCC operation of NGCC	design of PV/WT/BAT operation of all technologies	design of PCC/PV/WT/BAT operation of all technologies	design of PCC/PV/WT/BAT operation of all technologies

Table 7
Key assumptions of the case study for the province of Zeeland.

Efficiencies		
$\eta^{electricity}_{gas\ cycle}$	35.7	%
$\eta^{heat}_{gas\ cycle}$	54.6	%
$\eta_{steam\ cycle}$	38.0	%
Cost		
CO_2 emission	25	EUR/t_{CO2}
Gas import	0.03	EUR/kWh
NGCC (equipment)	123	kEUR/(MW y)
WT	335	kEUR/(MW_p y)
PV	405	kEUR/(MW_p y)
BAT	150	kEUR/MWh_p
Electricity		
Demand	3225	GWh/y
Cost (import)	0.067	EUR/kWh
Emission factor (import)	350.6	kg/MWh

each line is therefore infeasible. Note that the base case (only NGCC) is identified by a single point, which has the minimum cost but the highest emissions, as expected. Details about the design of each data point along the lines are reported in Table 8. When comparing the Pareto fronts of the scenarios with and without PCC, it is clear that adding a PCC unit to the system allows for cheaper decarbonisation. This is in line with earlier findings [58–60]. A key reason behind this result is that the NGCC unit is present in all scenarios, and its annuitised equipment costs must be accounted for, even if the capacity factor drastically decreases. This resembles cases of decarbonising an energy system where the fossil generation has newly been installed, and discontinuing it before the end of its lifetime would lead to significant economic losses. An interesting recent analysis of the costs and ownership of fossil fuels stranded assets, which is often neglected in energy system analysis, is reported in Semieniuk et al. [61]. As a consequence, it is cheaper to add a PCC unit (we find capture costs of ~40 EUR/t_{CO2}, which is in line with literature values for Nth-of-a-kind plants of 43 USD/t_{CO2} [62]) than to replace the complete production capacity of the NGCC with renewables while still accounting for the NGCC investment. It has to be noted that this finding shall not be generalised, as it depends heavily on the specific regional conditions, e.g. cost assumptions, the projected lifetime of the PCC unit, and the remaining lifetime of the NGCC unit.

Another interesting finding is that, except for the zero-emission design (and close-to-zero), renewable energy technologies are not chosen by the optimisation when PCC can be installed, i.e. the lowest cost of CO_2 abatement is achieved by using the NGCC plant in combination with CCS. This is also found in the case where PCC has a fast transition period of only one hour (PCC-fast); in other terms, higher PCC flexibility is not conducive to different technology combinations. While this might change for a different cost ratio between the different technologies, investigating this trade-off is beyond the scope of this work.

Comparing the Pareto fronts of the two scenarios with PCC would suggest that the constrained dynamics of the PCC unit have no effect on the system. A closer look at the operation, however, reveals significant differences (see Fig. 10). Fig. 10a shows that the operation profile of the PCC unit consists of a set of constant segments. This is caused by the steady-state period that the PCC unit has to maintain after each change of operation state and before the next: In order to fulfil the end-user demand, the NGCC cannot always limit itself to this pattern. Hence, part of the NGCC flue gas needs to be bypassed and emitted at certain times. Overall, however, this effect is limited and reduces the effective carbon capture rate to 89.5%. Fig. 10b shows that less CO_2 is bypassed when faster PCC dynamic is possible, and the gas turbine operation as a whole (seen by the total CO_2 as a proxy) becomes more flexible. While the effect on the effective carbon capture rate is limited (89.8%), the impact on the battery design and operation is significant (see Fig. 10c–d). With the originally constrained dynamics, the battery is in much higher demand since it has to compensate for the lack of flexibility imposed by the PCC for low-carbon power production. If the PCC, and consequentially the NGCC, could operate more flexibly, the required battery size would be halved (Fig. 10d). However, because of the high share of the NGCC plant cost over the total costs, this effect does not displace the Pareto fronts strongly.

Table 8
Installed technology capacities for the Pareto-optimal designs shown in Fig. 9.

			Emissions [kg_{CO2}/kWh]	Cost [EUR/kWh]	NGCC [MW]	WT [units]	PV [km^2]	Battery [MWh]	PCC [kmol/s]
NGCC	renewables		0	0.534	571	523	2.90	29 766	–
			0.044	0.239	571	221	4.30	6648	–
			0.087	0.171	571	189	2.00	3031	–
			0.175	0.100	571	109	0	527	–
			0.261	0.088	571	50	0.05	16.3	–
			0.349	0.076	571	0	0.01	0	–
NGCC	renewables	PCC	0	0.534	571	523	2.90	29 766	0
			0.044	0.092	571	0	0	131	32.5
			0.087	0.087	571	0	0	0	23.2
			0.175	0.083	571	0	0	0	14.9
			0.262	0.080	571	0	0	0	7.52
			0.349	0.076	571	0	0.05	0	0
NGCC	renewables	PCC (fast)	0	0.534	571	523	2.90	29 766	0
			0.044	0.091	571	0	0	59.1	33.3
			0.087	0.087	571	0	0	0.35	23.3
			0.175	0.083	571	0	0	0	15.0
			0.262	0.080	571	0	0	0	7.68
			0.349	0.076	571	0	0.05	0	0

4. Discussion

Naturally, every model has its limitations. In the current work, we see four limitations that should be highlighted. First, the CO_2 conditioning, e.g. purification, compression, or liquefaction, is not included in the model. This deliberate decision was taken because the conditioning depends on the end-use and the model is intended to be universally applicable. This implies that, when combining various technology models to a system model, the conditioning process needs to be considered as a separate model as well. This is especially important since the conditioning process might add additional constraints to the dynamic operation of the whole system. Second, amine degradation was not considered. In reality, this effect would lead to an increase in OPEX and/or a decrease in performance over time. The capture performance itself is less of a problem since (a) degraded MEA can be compensated with fresh MEA and (b) the degradation products have a certain ability to capture CO_2 as well [63]. However, the degradation products might affect the heat transfer properties and, consequentially, lead to an increase in the reboiler duty [64]. Furthermore, frequently ramping up and down might increase the degradation rate [64]. Third, the capture rate is assumed to be constant at 90% even during ramping operations. If one desires to include different carbon capture rates for the different operation modes (steady-state, ramp up, and ramp down), the binary indicators for ramping operations may be used to switch between different carbon capture rates. Note, however, that this causes another bilinearity between the flue gas flow rate and the binary indicators, the effect of which has not been investigated in this work. Moreover, the parameters of the dynamic constraints implicitly assume a certain control strategy and, consequentially, operational limits which cannot be violated by the model. While an analysis of a carbon capture plant's performance when violating these operational limits is not possible with the current model formulation, other operational limits can be tested by adjusting the parameters TP and ν to change the transition period and the ramping limit, respectively. The final limitation of this work lies in the cost data. While the data used for this model agrees with other studies in the open literature, no information about how costs will develop (e.g. learning curves) were implemented. This has two implications: (a) the model cannot be directly used for multi-decade analyses and (b) the parameters of the cost model need to be updated when significant costs improvements occur.

5. Conclusions

In this work, we presented a mixed integer linear model of an MEA-based post-combustion capture process. Three aspects make it go beyond existing literature. First, it allows to transfer information from detailed process simulations – including rate-based modelling and the full capture process – to the mixed-integer linear framework. This results in a reliable and accurate linear model. Second, the model is portable to many different boundary conditions and applications. This was achieved via embedding the effect of variations in CO_2 concentration and flow rate on both the energetic performance and the costs. Third, it considers constraints describing the dynamic behaviour of the unit. Combining these three aspects makes it possible to apply the model in most energy system design and optimisation frameworks and allows us to answer questions like which streams to capture from, how to size the plant, and how to operate the plant. This ability places the model right in the gap between detailed, plant-level models like the one presented by Zantye et al. [26,27] and top-level system models like TIMES [12], OSeMOSYS [14], or OPERA [13].

The model was validated with real plant data at different levels throughout the development: from the validation of the rate-based model of the absorber and the full capture process with pilot plant data to the comparison of the MILP model with Petra Nova plant data. The latter point makes the MILP model particularly valuable for large-scale energy/process system optimisation.

The capabilities of the model were demonstrated with a case study in which an NGCC-based energy system was to be decarbonised. The flexibility of the carbon capture model allowed us to gain insights into the response of the unit to flexible NGCC operation as well as the impact of renewable energy sources on the system.

In a sensitivity analysis of the model's performance parameters, it was shown that variations of the parameter β, i.e. the parameter multiplying the CO_2 concentration, have the most influence. Hence, this parameter should be the number one priority when aiming at high model accuracy. However, analysing the effect on commonly used KPIs revealed that the ultimate effect of uncertainties of the performance parameters highly depends on the application. In particular, applications with abundant waste heat are the most resilient since they can easily buffer variations in the heat demand of the carbon capture unit.

Based on the identified limitations, we see three developments for future research. First, deriving a portfolio of the most common conditioning processes will make the model more user-friendly and, therefore, more universally applicable. Second, since our model already includes constraints on the plant's dynamic behaviour, it would lend itself well to investigate the effect of amine degradation on the performance of a larger energy system. However, amine degradation is influenced by many factors. Hence, including this feature would most likely require to model discrete scenarios which limits the generality

of the model. Finally, backing the cost parameters with learning curves will make the cost model more resilient to changes over time and allows to analyse multi-decade time horizons as well — if computation time allows for it.

Data availability

Data will be made available on request.

Acknowledgements

ACT ELEGANCY, Project No 271498, has received funding from DETEC (CH), FZJ/PtJ (DE), RVO (NL), Gassnova (NO), BEIS (UK), Gassco AS and Statoil Petroleum AS, and is cofunded by the European Commission under the Horizon 2020 programme, ACT Grant Agreement No 691712.

Appendix A. Supplementary data

Supplementary material related to this article can be found online at https://doi.org/10.1016/j.apenergy.2023.120738.

References

[1] Sgouridis S, Carbajales-Dale M, Csala D, Chiesa M, Bardi U. Comparative net energy analysis of renewable electricity and carbon capture and storage. Nat Energy 2019;4(6):456–65. http://dx.doi.org/10.1038/s41560-019-0365-7.

[2] Merk C, Nordø AD, Andersen G, Lægreid OM, Tvinnereim E. Don't send us your waste gases: Public attitudes toward international carbon dioxide transportation and storage in Europe. Energy Res Soc Sci 2022;87:102450. http://dx.doi.org/10.1016/J.ERSS.2021.102450.

[3] International Energy Agency. Net zero by 2050 - a roadmap for the global energy sector. Tech. rep., IEA; 2021.

[4] Intergovernmental Panel on Climate Change (IPCC). Global warming of 1.5 ºC. Tech. rep., IPCC; 2018.

[5] Bui M, Gazzani M, Pozo C, Puxty GD, Soltani SM. Editorial: The role of carbon capture and storage technologies in a net-zero carbon future. Front Energy Res 2021;9:565. http://dx.doi.org/10.3389/FENRG.2021.733968.

[6] Intergovernmental Panel on Climate Change (IPCC). Climate change 2022 - working group III contribution to the sixth assessment report of the intergovernmental panel on climate change. Tech. rep., IPCC; 2022.

[7] Bischi A, Taccari L, Martelli E, Amaldi E, Manzolini G, Silva P, et al. A detailed MILP optimization model for combined cooling, heat and power system operation planning. Energy 2014;74(C):12–26. http://dx.doi.org/10.1016/J.ENERGY.2014.02.042.

[8] Weimann L, Gabrielli P, Boldrini A, Kramer GJ, Gazzani M. Optimal hydrogen production in a wind-dominated zero-emission energy system. Adv Appl Energy 2021;3:100032. http://dx.doi.org/10.1016/J.ADAPEN.2021.100032.

[9] Ahmetović E, Kravanja Z, Ibrić N, Grossmann IE, Savulescu LE. State of the art methods for combined water and energy systems optimisation in Kraft pulp mills. Opt Eng 2021;22(3):1831–52. http://dx.doi.org/10.1007/S11081-021-09612-4.

[10] Ye Y, Grossmann IE, Pinto JM. Mixed-integer nonlinear programming models for optimal design of reliable chemical plants. Comput Chem Eng 2018;116:3–16. http://dx.doi.org/10.1016/J.COMPCHEMENG.2017.08.013.

[11] Moretti L, Manzolini G, Martelli E. MILP and MINLP models for the optimal scheduling of multi-energy systems accounting for delivery temperature of units, topology and non-isothermal mixing. Appl Therm Eng 2021;184. http://dx.doi.org/10.1016/J.APPLTHERMALENG.2020.116161.

[12] Loulou R, Remne U, Kanudia A, Lehtila A, Goldstein G. Documentation for the TIMES model - part I. Tech. rep., IEA-ETSAP; 2005, URL https://iea-etsap.org/docs/Documentation_for_the_TIMES_Model-Part-I_July-2016.pdf. Accessed 12 Feb. 2023.

[13] van Stralen JN, Dalla Longa F, Daniëls BW, Smekens KE, van der Zwaan B. OPERA: a new high-resolution energy system model for sector integration research. Environ Model Assess 2021;26(6):873–89. http://dx.doi.org/10.1007/S10666-020-09741-7.

[14] Henke HT, Gardumi F, Howells M. The open source electricity model base for Europe - an engagement framework for open and transparent European energy modelling. Energy 2022;239. http://dx.doi.org/10.1016/J.ENERGY.2021.121973.

[15] Connolly D, Lund H, Mathiesen BV, Leahy M. A review of computer tools for analysing the integration of renewable energy into various energy systems. Appl Energy 2010;87(4):1059–82. http://dx.doi.org/10.1016/J.APENERGY.2009.09.026.

[16] Pfenninger S, Hawkes A, Keirstead J. Energy systems modeling for twenty-first century energy challenges. Renew Sustain Energy Rev 2014;33:74–86. http://dx.doi.org/10.1016/J.RSER.2014.02.003.

[17] Bui M, Adjiman CS, Bardow A, Anthony EJ, Boston A, Brown S, et al. Carbon capture and storage (CCS): the way forward. Energy Environ Sci 2018;11(5):1062–176. http://dx.doi.org/10.1039/C7EE02342A.

[18] Zhang S, Liu L, Zhang L, Zhuang Y, Du J. An optimization model for carbon capture utilization and storage supply chain: A case study in Northeastern China. Appl Energy 2018;231:194–206. http://dx.doi.org/10.1016/J.APENERGY.2018.09.129.

[19] Zhang S, Zhuang Y, Tao R, Liu L, Zhang L, Du J. Multi-objective optimization for the deployment of carbon capture utilization and storage supply chain considering economic and environmental performance. J Clean Prod 2020;270:122481. http://dx.doi.org/10.1016/J.JCLEPRO.2020.122481.

[20] Li K, Shen S, Fan JL, Xu M, Zhang X. The role of carbon capture, utilization and storage in realizing China's carbon neutrality: A source-sink matching analysis for existing coal-fired power plants. Resour Conserv Recy 2022;178:106070. http://dx.doi.org/10.1016/J.RESCONREC.2021.106070.

[21] d'Amore F, Mocellin P, Vianello C, Maschio G, Bezzo F. Economic optimisation of European supply chains for CO2 capture, transport and sequestration, including societal risk analysis and risk mitigation measures. Appl Energy 2018;223:401–15. http://dx.doi.org/10.1016/J.APENERGY.2018.04.043.

[22] d'Amore F, Sunny N, Iruretagoyena D, Bezzo F, Shah N. European supply chains for carbon capture, transport and sequestration, with uncertainties in geological storage capacity: Insights from economic optimisation. Comput Chem Eng 2019;129:106521. http://dx.doi.org/10.1016/J.COMPCHEMENG.2019.106521.

[23] Chung W, Lee JH. Input-output surrogate models for efficient economic evaluation of amine scrubbing CO2capture processes. Ind Eng Chem Res 2020;59(42):18951–64. http://dx.doi.org/10.1021/acs.iecr.0c02971.

[24] Wiesberg IL, de Medeiros JL, Paes de Mello RV, Santos Maia JG, Bastos JBV, Araújo OdQF. Bioenergy production from sugarcane bagasse with carbon capture and storage: Surrogate models for techno-economic decisions. Renew Sustain Energy Rev 2021;150:111486. http://dx.doi.org/10.1016/J.RSER.2021.111486.

[25] Bassano C, Deiana P, Vilardi G, Verdone N. Modeling and economic evaluation of carbon capture and storage technologies integrated into synthetic natural gas and power-to-gas plants. Appl Energy 2020;263:114590. http://dx.doi.org/10.1016/J.APENERGY.2020.114590.

[26] Zantye MS, Arora A, Hasan MM. Renewable-integrated flexible carbon capture: a synergistic path forward to clean energy future. Energy Environ Sci 2021;14(7):3986–4008. http://dx.doi.org/10.1039/D0EE03946B.

[27] Zantye MS, Arora A, Faruque Hasan MM. Operational power plant scheduling with flexible carbon capture: A multistage stochastic optimization approach. Comput Chem Eng 2019;130:106544. http://dx.doi.org/10.1016/J.COMPCHEMENG.2019.106544.

[28] Zhang X, Bai Y, Zhang Y. Collaborative optimization for a multi-energy system considering carbon capture system and power to gas technology. Sustain Energy Technol Assess 2022;49:101765. http://dx.doi.org/10.1016/J.SETA.2021.101765.

[29] Ma Y, Wang H, Hong F, Yang J, Chen Z, Cui H, et al. Modeling and optimization of combined heat and power with power-to-gas and carbon capture system in integrated energy system. Energy 2021;236:121392. http://dx.doi.org/10.1016/J.ENERGY.2021.121392.

[30] Dong W, Lu Z, He L, Geng L, Guo X, Zhang J. Low-carbon optimal planning of an integrated energy station considering combined power-to-gas and gas-fired units equipped with carbon capture systems. Int J Electr Power Energy Syst 2022;138:107966. http://dx.doi.org/10.1016/J.IJEPES.2022.107966.

[31] Weimann L, Dubbink G, van der Ham L, Kramer GJ, Gazzani M. An MILP model of post-combustion carbon capture based on detailed process simulation. Comput Aided Chem Eng 2021;50:319–25. http://dx.doi.org/10.1016/B978-0-323-88506-5.50051-6.

[32] Gabrielli P, Gazzani M, Martelli E, Mazzotti M. Optimal design of multi-energy systems with seasonal storage. Appl Energy 2018;219:408–24. http://dx.doi.org/10.1016/j.apenergy.2017.07.142.

[33] Gabrielli P, Gazzani M, Mazzotti M. Electrochemical conversion technologies for optimal design of decentralized multi-energy systems: Modeling framework and technology assessment. Appl Energy 2018;221:557–75. http://dx.doi.org/10.1016/j.apenergy.2018.03.149.

[34] Liang ZH, Rongwong W, Liu H, Fu K, Gao H, Cao F, et al. Recent progress and new developments in post-combustion carbon-capture technology with amine based solvents. Int J Greenh Gas Control 2015;40:26–54. http://dx.doi.org/10.1016/J.IJGGC.2015.06.017.

[35] Chao C, Deng Y, Dewil R, Baeyens J, Fan X. Post-combustion carbon capture. Renew Sustain Energy Rev 2021;138:110490. http://dx.doi.org/10.1016/J.RSER.2020.110490.

[36] Amirkhosrow M, Pérez-Calvo J-F, Gazzani M, Mazzotti M, Lay EN. Rigorous rate-based model for CO2 capture via monoethanolamine-based solutions: effect of kinetic models, mass transfer, and holdup correlations on prediction accuracy. Sep Sci Technol 2021;56(9):1491–509. http://dx.doi.org/10.1080/01496395.2020.1784943.

[37] Aboudheir A, Tontiwachwuthikul P, Chakma A, Idem R. Kinetics of the reactive absorption of carbon dioxide in high CO2-loaded, concentrated aqueous monoethanolamine solutions. Chem Eng Sci 2003;58(23–24):5195–210. http://dx.doi.org/10.1016/J.CES.2003.08.014.

[38] Bravo JL, Rocha JA, Fair JR. Mass transfer in gauze packings. Hydrocarbon Process (Int Ed) 1985;64(1).

[39] Zhang Q, Turton R, Bhattacharyya D. Development of model and model-predictive control of an MEA-based postcombustion CO2 capture process. Ind Eng Chem Res 2016;55(5):1292–308. http://dx.doi.org/10.1021/ACS.IECR.5B02243.

[40] Notz R, Mangalapally HP, Hasse H. Post combustion CO2 capture by reactive absorption: Pilot plant description and results of systematic studies with MEA. Int J Greenh Gas Control 2012;6:84–112. http://dx.doi.org/10.1016/j.ijggc.2011.11.004.

[41] Mitsubishi Heavy Industries. MHI's carbon capture technology. 2017, URL https://www.co2conference.net/wp-content/uploads/2017/12/4-MHI-Slides-on-the-PetroNova-Project.pdf. Accessed 12 Feb. 2023.

[42] Armpriester A. W.A. Parish Post-Combustion CO2 capture and sequestration project. Tech. rep., Petra Nova Parish Holdings; 2017, https://www.osti.gov/biblio/1344080. Accessed 12 Feb. 2023.

[43] Kennedy G. W.A. parish post-combustion CO2 capture and sequestration demonstration project (final technical report). Tech. rep., Pittsburgh, PA, Morgantown, WV (United States): National Energy Technology Laboratory; 2020, http://dx.doi.org/10.2172/1608572.

[44] TNO. CO2 capture with AVR. 2021, URL https://www.tno.nl/en/focus-areas/energy-transition/roadmaps/towards-co2-neutral-industry/reducing-co2-emissions-through-capture-use-and-storage/co2-capture-with-avr/. Accessed 12 Feb. 2023.

[45] Luyben WL. Distillation design and control using aspen™ simulation. John Wiley & Sons, Inc. 2013, http://dx.doi.org/10.1002/9781118510193.

[46] Bui M, Flø NE, de Cazenove T, Mac Dowell N. Demonstrating flexible operation of the technology centre mongstad (TCM) CO2 capture plant. Int J Greenh Gas Control 2020;93:102879. http://dx.doi.org/10.1016/J.IJGGC.2019.102879.

[47] Marx-Schubach T, Schmitz G. Dynamic simulation and investigation of the startup process of a postcombustion-capture plant. Ind Eng Chem Res 2018;57(49):16751–62. http://dx.doi.org/10.1021/acs.iecr.8b03444.

[48] Tait P, Buschle B, Milkowski K, Akram M, Pourkashanian M, Lucquiaud M. Flexible operation of post-combustion CO2 capture at pilot scale with demonstration of capture-efficiency control using online solvent measurements. Int J Greenh Gas Control 2018;71:253–77. http://dx.doi.org/10.1016/J.IJGGC.2018.02.023.

[49] Marx-Schubach T, Schmitz G. Optimizing the start-up process of post-combustion capture plants by varying the solvent flow rate. In: Proceedings of the 12th international modelica conference. Vol. 132. Linköping University Electronic Press; 2017, p. 121–30. http://dx.doi.org/10.3384/ECP17132121.

[50] Hasan MM, Baliban RC, Elia JA, Floudas CA. Modeling, simulation, and optimization of postcombustion CO2 capture for variable feed concentration and flow rate. 1. Chemical absorption and membrane processes. Ind Eng Chem Res 2012;51(48):15642–64. http://dx.doi.org/10.1021/IE301571D.

[51] Aromada SA, Eldrup NH, Erik Øi L. Capital cost estimation of CO2 capture plant using Enhanced Detailed Factor (EDF) method: Installation factors and plant construction characteristic factors. Int J Greenh Gas Control 2021;110:103394. http://dx.doi.org/10.1016/J.IJGGC.2021.103394.

[52] Markewitz P, Zhao L, Ryssel M, Moumin G, Wang Y, Sattler C, et al. Carbon capture for CO2 emission reduction in the cement industry in Germany. Energies 2019;12(12):2432. http://dx.doi.org/10.3390/EN12122432.

[53] Glover F. Improved linear integer programming formulations of nonlinear integer problems. Vol. 22. No. 4. INFORMS; 1975, p. 455–60. http://dx.doi.org/10.1287/MNSC.22.4.455.

[54] Anantharaman R, Fu C, Roussanaly S, Voldsund M. D4.2 - Design and performance of CEMCAP cement plant with MEA post combustion capture. Tech. Rep., SINTEF Energi AS; 2016.

[55] IEA Greenhouse Gas R&D Programme. CO2 capture in the cement industry. Tech. Rep., International Energy Agency; 2008.

[56] Anantharaman R, Bolland O, Booth N, van Dorst E, Ekstrom C, Sanchez Fernandez E, et al. D4.9 - European best practice guidelines for assessment of CO2 capture technologies. Tech. Rep., CAESAR; 2011.

[57] Weimann L, Gazzani M. A novel time discretization method for solving complex multi-energy system design and operation problems with high penetration of renewable energy. Comput Chem Eng 2022;163:107816. http://dx.doi.org/10.1016/J.COMPCHEMENG.2022.107816.

[58] Baylin-Stern A, Berghout N. Is carbon capture too expensive? – Analysis - IEA. 2021, URL https://www.iea.org/commentaries/is-carbon-capture-too-expensive. Accessed 12 Feb. 2023.

[59] Heuberger CF, Staffell I, Shah N, Mac Dowell N. Quantifying the value of CCS for the future electricity system. Energy Environ Sci 2016;9(8):2497–510. http://dx.doi.org/10.1039/C6EE01120A.

[60] Lau HC, Ramakrishna S, Zhang K, Radhamani AV. The role of carbon capture and storage in the energy transition. Energy Fuels 2021;35(9):7364–86. http://dx.doi.org/10.1021/ACS.ENERGYFUELS.1C00032.

[61] Semieniuk G, Holden PB, Mercure J-F, Salas P, Pollitt H, Jobson K, et al. Stranded fossil-fuel assets translate to major losses for investors in advanced economies. Nat Clim Chang 2022;12(6):532–8. http://dx.doi.org/10.1038/s41558-022-01356-y.

[62] Irlam L. Global costs of carbon capture and storage 2017 update. Tech. Rep., Global CCS Institute; 2017.

[63] Zoannou KS, Sapsford DJ, Griffiths AJ. Thermal degradation of monoethanolamine and its effect on CO2 capture capacity. Int J Greenh Gas Control 2013;17:423–30. http://dx.doi.org/10.1016/J.IJGGC.2013.05.026.

[64] Flø NE, Faramarzi L, De Cazenove T, Hvidsten OA, Morken AK, Hamborg ES, et al. Results from MEA degradation and reclaiming processes at the CO2 technology centre mongstad. Energy Procedia 2017;114:1307–24. http://dx.doi.org/10.1016/J.EGYPRO.2017.03.1899.